Available online at www.sciencedirect.com
ScienceDirect
Journal of Catalysis 255 (2008) 269–278
JOURNAL OF CATALYSIS
www.elsevier.com/locate/jcat

Low-temperature CO oxidation over $Au/ZnO/SiO_2$ catalysts: Some mechanism insights

Kun Qian [a], Weixin Huang [a,*], Jun Fang [a], Shanshan Lv [a], Bo He [b], Zhiquan Jiang [a], Shiqiang Wei [b]

[a] *Hefei National Laboratory for Physical Sciences at the Microscale and Department of Chemical Physics, University of Science and Technology of China, Hefei 230026, China*
[b] *National Synchrotron Radiation Laboratory, University of Science and Technology of China, Hefei 230029, China*

Received 7 November 2007; revised 16 February 2008; accepted 19 February 2008

Available online 24 March 2008

Abstract

We report a new type of supported Au catalyst active in low-temperature CO oxidation. $Au/ZnO/SiO_2$ catalysts were prepared by routine deposition–precipitation with ammonium hydroxide ($Au/ZnO/SiO_2$-NH_3) and aqueous solution of Na_2CO_3 ($Au/ZnO/SiO_2$-Na_2CO_3) as the precipitation agent. The catalysts were characterized by BET surface area, X-ray diffraction, transmission electron microscopy, X-ray photoemission spectroscopy, photoluminescence spectroscopy, and X-ray absorption spectroscopy. $Au/ZnO/SiO_2$-Na_2CO_3 is more active than $Au/ZnO/SiO_2$-NH_3, achieving a complete CO conversion at 303 K. The structures of Au nanoparticles and ZnO are strongly affected by the Au–ZnO interaction in $Au/ZnO/SiO_2$ catalysts. The Au–ZnO interaction is stronger, and thus the Au nanoparticles are more highly dispersed in $Au/ZnO/SiO_2$-Na_2CO_3 than in $Au/ZnO/SiO_2$-NH_3. Our results suggest that CO oxidation catalyzed by supported Au nanoparticles follows different mechanisms at low and high reaction temperatures and that a weakly chemisorbed species is involved in low-temperature CO oxidation.

Keywords: $Au/ZnO/SiO_2$ catalyst; CO oxidation; Reaction mechanism; Metal–support interaction

1. Introduction

Low-temperature CO oxidation catalyzed by supported Au nanoparticles has rapidly become a hot topic both fundamentally and practically [1–4] since Haruta et al. reported that fine Au nanoparticles supported on TiO_2 were active in low-temperature CO oxidation [5]. Although great success has been achieved on the synthesis of supported Au catalysts active in low-temperature CO oxidation, the reaction mechanism remains ambiguous. Haruta and Daté [2] proposed multiple reaction pathways for CO oxidation over Au/TiO_2 catalyst, including the direct reaction between CO adsorbed on Au and O_2^- adsorbed on TiO_2 at the perimeter sites. Another popular reaction mechanism involves the insertion of an adsorbed CO into an Au–OH bond to form a hydroxycarbonyl that is oxidized to bicarbonate, which then decomposes into Au–OH and CO_2 [6,7]. The active site in this reaction mechanism consists of an ensemble of metallic Au atoms with a Au cation (Au(I) or Au(III)) at the periphery with a hydroxyl ligand. A general observation of the structure–activity relationship in supported Au catalysts for low-temperature CO oxidation is the size-dependent activity. The oxide support plays a crucial role in determining the activity of Au catalysts. Schubert et al. grouped various oxide supports into two categories: inert supports (SiO_2, Al_2O_3, and MgO) and active supports (reducible transitional metal oxides such as TiO_2, CoO_x, CeO_2, and Fe_2O_3) [8]. They based this classification on the observation that Au nanoparticles supported on inert oxides exhibited lower intrinsic activities than those supported on active oxides that can contribute to the activation and supply of oxygen for the reaction. It also was found that fine Au nanoparticles could be easily prepared on reducible oxide supports through the routine methods of coprecipitation and deposition–precipitation (DP) using $HAuCl_4$ as the precursor, but that this approach usually led to the formation of relatively large Au nanoparticles on Al_2O_3 and SiO_2 [8]. Therefore, Au/SiO_2 catalysts prepared by coprecipitation or DP using $HAuCl_4$ as the precursor exhibit poor catalytic performance in

* Corresponding author. Fax: +86 551 3600437.
E-mail address: huangwx@ustc.edu.cn (W.X. Huang).

0021-9517/$ – see front matter
doi:10.1016/j.jcat.2008.02.012

CO oxidation, usually becoming active at reaction temperatures above 573 K [9–13].

Preparation of Au/SiO_2 catalysts active in low-temperature CO oxidation is of great interest, however. Practically, SiO_2 is one of the favorite supports for industrial catalysts because of its high thermal stability and mechanical strength; fundamentally, active Au/SiO_2 catalysts can help elucidate the active structure and reaction mechanism in low-temperature CO oxidation related only to Au because of the inertness of SiO_2. Au/SiO_2 catalysts active in CO oxidation at room temperature or even lower temperatures have been successfully prepared by chemical vapor deposition (CVD) [9,14], using gold inorganic–organic high-surface area materials [15] and the cationic Au complex ($Au(en)_2Cl_3$) as precursors [16,17]. These results demonstrate that supported fine Au nanoparticles can catalyze low-temperature CO oxidation without the involvement of oxide supports. But the aforementioned synthesis routes of active Au/SiO_2 catalysts involve either complicate procedures or uncommon Au compounds, which might hamper their large-scale applications.

We recently found that fine Au nanoparticles can be easily prepared on a CoO_x-modified SiO_2 surface by DP using $HAuCl_4$ as the precursor and are active in low-temperature CO oxidation [18]. "Active" oxides have been used as additives to enhance the catalytic activity of Au/SiO_2 catalysts in CO oxidation. Dekkers et al. investigated the effect of "active"-oxide additives (CoO_x, LaO_x, CeO_x) on the activity of Au/SiO_2 catalysts, but found no enhanced effect in low-temperature CO oxidation under their experimental conditions [10]. Guczi et al. investigated a $FeO_x/Au/SiO_2/Si(100)$ model catalyst and found that Au promoted the catalytic activity of FeO_x in CO oxidation [19]. Venezia et al. anchored Au nanoparticles on TiO_2/SiO_2 by the sol method and found that $Au/TiO_2/SiO_2$ catalysts with a TiO_2 loading below 5 wt% demonstrated better catalytic performance in CO oxidation than the similarly prepared Au/TiO_2 catalysts [20]. The interfacial structures of various $Au/TiO_2/SiO_2$ catalysts also have been investigated in detail [21]. Recently, Zhu et al. reported the effects of various oxide additives (some negative, others positive) on the catalytic activity of Au/SiO_2 in CO oxidation, in which Au/SiO_2 catalysts were prepared using $Au(en)_2Cl_3$ as the precursor [17].

The $Au/CoO_x/SiO_2$ catalyst that we reported earlier might be of potential practical applications because of its convenient preparation method [18]. In the present work, we used our synthesis strategy to prepare $Au/ZnO/SiO_2$ catalysts active in low-temperature CO oxidation. ZnO does not belong to the reducible oxides, but Au/ZnO catalysts have been demonstrated to be active in low-temperature CO oxidation [22,23]. In this work, we take the unique advantage of the $Au/ZnO/SiO_2$ catalyst to investigate the structure–activity relationship of Au/ZnO catalysts in low-temperature CO oxidation. In $Au/ZnO/SiO_2$, the inert SiO_2 is the major component, and the loadings of active components Au and ZnO are comparable; thus, the Au–ZnO interaction and its influence on the structure and activity of the catalyst can be manifested. Our results demonstrate that the stronger the Au–ZnO interaction, the finer the supported Au nanoparticles, and the better the catalytic performance of the catalyst in low-temperature CO oxidation. Our results also suggest that CO oxidation over $Au/ZnO/SiO_2$ follows different reaction mechanisms at low and high reaction temperatures and that a weakly chemisorbed species is involved in the low-temperature CO oxidation.

2. Experimental

2.1. Catalyst preparation

Typically, SiO_2 (40–120 mesh, Qingdao Haiyang Chemicals Co.) was first modified with 6% ZnO (Zn/SiO_2 weight ratio) by the conventional incipient wetness impregnation (using $Zn(NO_3)_2{\cdot}6H_2O$ (Sinopharm Chemical Reagent Co., Ltd; $\geqslant$99.0%) as the zinc precursor), followed by drying at 60 °C and calcination at 200 °C. The resulting ZnO/SiO_2 was then used to prepare the 2% Au/6% ZnO/SiO_2 (Au/SiO_2 weight ratio) catalyst by DP using $HAuCl_4{\cdot}4H_2O$ (Sinopharm Chemical Reagent Co., Ltd; Au content $\geqslant$47.8%) as the precursor. The $HAuCl_4{\cdot}4H_2O$ aqueous solution and the DP agent were slowly co-added into a three-necked bottle containing ZnO/SiO_2, with the pH controlled between 9 and 10. The system was stirred at 60 °C for 24 h, after which the solid was filtered and washed several times. The resulting powder was dried at 60 °C for 24 h, followed by calcination at 200 °C for 4 h. In our experiments, ammonium hydroxide and aqueous solution of Na_2CO_3 were used as the DP agent, and the resulting catalysts were designated $Au/ZnO/SiO_2$-NH_3 and $Au/ZnO/SiO_2$-Na_2CO_3. The 2% Au/SiO_2 (designated Au/SiO_2) and 6% ZnO/SiO_2 (designated ZnO/SiO_2) catalysts were prepared similarly for comparison purposes.

2.2. Catalyst characterization

BET surface areas were acquired on a Beckman Coulter SA3100 surface area analyzer, in which the sample was degassed at 120 °C for 30 min in nitrogen atmosphere before the measurements. Powder X-ray diffraction (XRD) patterns were acquired on a Philips X'Pert PRO SUPER X-ray diffractometer with a Ni-filtered Cu$K\alpha$ X-ray source operating at 40 kV and 50 mA. High resolution X-ray photoelectron spectroscopy (XPS) measurements were performed on an ESCALAB 250 high-performance electron spectrometer using a monochromatized Al$K\alpha$ excitation source ($h\nu = 1486.6$ eV). The binding energies in XPS spectra were referenced with respect to the Si 2p binding energy in SiO_2 at 103.3 eV. The photoluminescence (PL) spectra were acquired on a Fluorolog-Tau-3 steady-state/lifetime spectrofluorometer. Transmission electron microscopy (TEM) experiments were preformed on a JEOL 2010 high-resolution transmission electron microscope with an energy dispersive spectrum (EDS) analysis facility. The compositions of catalysts were analyzed by inductively coupled plasma atomic emission spectrometry (ICP-AES).

X-ray absorption spectroscopy (XAS) measurements for the Au L_{III}-edge (11,719–12,919 eV) and the Zn K-edge (9460–10,660 eV) were performed in the fluorescence mode at room temperature on the XAFS Station of the U7C beam line of

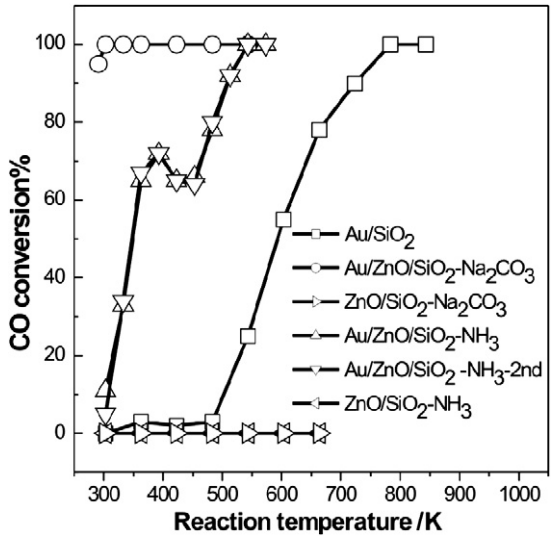

Fig. 1. Catalytic performances of various catalysts in CO oxidation.

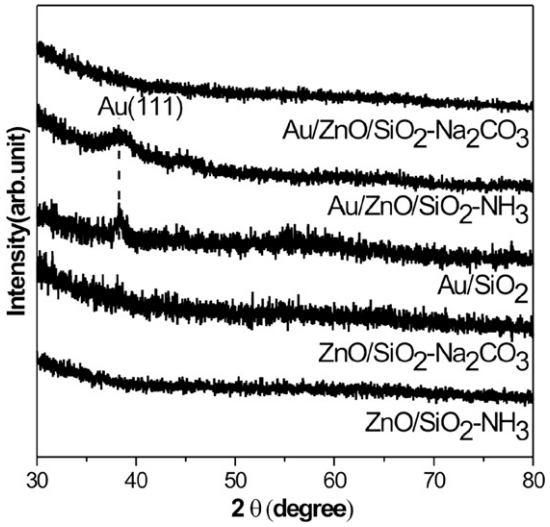

Fig. 2. XRD patterns of various catalysts.

National Synchrotron Radiation Laboratory (NSRL, Hefei, China). The synchrotron radiation facility consists mainly of an 800-MeV electron storage ring with the ring current of about 100–300 mA. A Si(111) double-crystal was used as the monochromator. The X-ray absorption near-edge structure (XANES) spectra were acquired at 1-eV energy steps.

2.3. Catalytic activity measurement

The catalytic activity was evaluated with a fixed-bed flow reactor. The catalyst underwent no pretreatment before the catalytic reaction. The catalyst sample was 100 mg, and the reaction gas consisting of 1% CO and 99% dry air was fed at a rate of 20 mL/min. The composition of the effluent gas was detected with an online GC-14C gas chromatograph equipped with a TDX-01 column ($T = 80\,^{\circ}\mathrm{C}$, H_2 as the carrier gas at 30 mL/min). The CO conversion was calculated from the change in CO concentrations in the inlet and outlet gases.

3. Results

Fig. 1 shows the catalytic activities of various catalysts in CO oxidation. The bare SiO_2 support and ZnO/SiO_2 supports exhibited no activity in CO oxidation at the temperatures investigated. The Au/SiO_2 catalyst exhibited poor catalytic activity, becoming active at reaction temperatures above 543 K. Both $Au/ZnO/SiO_2$-NH_3 and $Au/ZnO/SiO_2$-Na_2CO_3 exhibited catalytic activity in low-temperature CO oxidation. $Au/ZnO/SiO_2$-Na_2CO_3 was more active, capable of completely converting CO at 303 K. The actual Au/SiO_2 and Zn/SiO_2 weight ratios in $Au/ZnO/SiO_2$-Na_2CO_3 were 1.12% and 6%, respectively, as determined by ICP-AES; therefore, $Au/ZnO/SiO_2$-Na_2CO_3 exhibited a specific rate of CO oxidation not lower than 0.464 $\mathrm{mol_{CO}\,g_{Au}^{-1}\,h^{-1}}$ at 303 K. An interesting observation is the activity–temperature dependence. With increasing reaction temperature, CO conversion remained at 100% for $Au/ZnO/SiO_2$-Na_2CO_3; however, $Au/ZnO/SiO_2$-NH_3 demonstrated an unexpected activity–temperature dependence, with CO conversion rising from 11% at 303 K to 72% at 393 K, then decreasing to a minimum of 66% at 453 K, and the eventually increasing again. The complete oxidation of CO catalyzed by $Au/ZnO/SiO_2$-NH_3 was achieved at reaction temperatures above 513 K. We reevaluated the used $Au/ZnO/SiO_2$-NH_3 catalyst and found that it exhibited the same catalytic activity and the same activity–temperature dependence as the fresh $Au/ZnO/SiO_2$-NH_3 catalyst. This result demonstrates that the active structure of $Au/ZnO/SiO_2$-NH_3 did not change during the course of CO oxidation, and thus that the observed activity–temperature dependence cannot be attributed to the structural variation of the catalyst.

Table 1 summarizes the BET surface areas and the actual catalyst compositions of Au/SiO_2, $Au/ZnO/SiO_2$-NH_3, and $Au/ZnO/SiO_2$-Na_2CO_3 analyzed by ICP-AES. The BET surface areas of SiO_2 and ZnO/SiO_2 were 390 and 280 m^2/g, respectively. The difference in the ZnO loading between $Au/ZnO/SiO_2$-NH_3 and $Au/ZnO/SiO_2$-Na_2CO_3 can be attributed to the likely partial dissolution of ZnO by the formation of a Zn–NH_3 complex during the course of DP using

Table 1
Macroscopic structure parameters of various catalysts

Catalyst	BET surface areas (m^2/g)	Weight ratio		Average size of Au particles (nm)	
		Au/SiO_2	Zn/SiO_2	d_{XRD}	d_{TEM}
Au-SiO_2	316	1.02%	–	12	10.4
$Au/ZnO/SiO_2$-NH_3	297	1.55%	4.8%	5	5.0
$Au/ZnO/SiO_2$-Na_2CO_3	254	1.12%	6.0%	n.d.[a]	3.7

[a] Not detected.

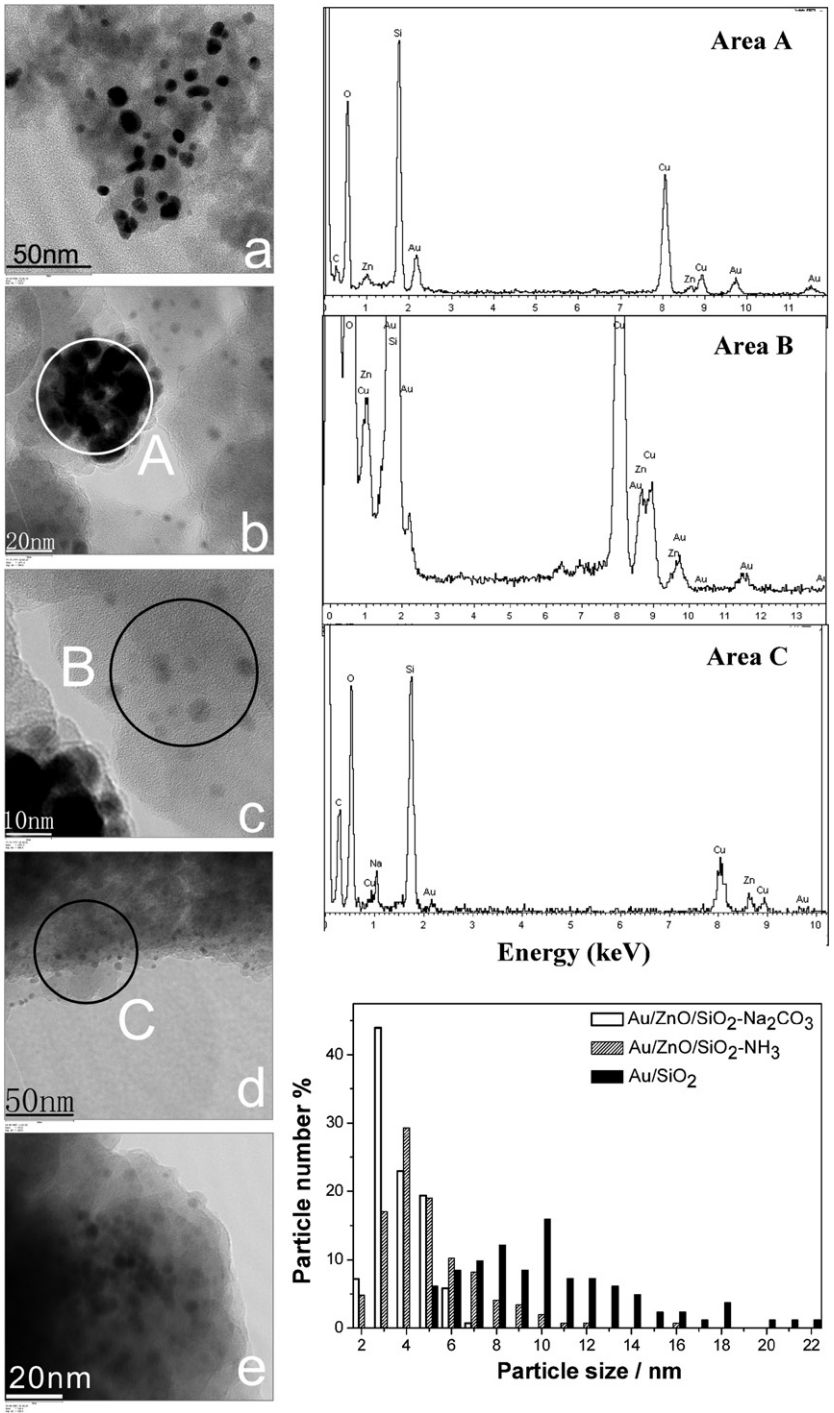

Fig. 3. (Left) TEM images of Au/SiO_2 (a), $Au/ZnO/SiO_2$-NH_3 (b, c), and $Au/ZnO/SiO_2$-Na_2CO_3 (d, e). (Right) EDS results of areas A, B, and C and size distributions of Au nanoparticles in Au/SiO_2, $Au/ZnO/SiO_2$-NH_3, and $Au/ZnO/SiO_2$-Na_2CO_3.

ammonium hydroxide. Fig. 2 shows XRD patterns of various catalysts. The XRD spectrum (not shown) demonstrates that calcining the unsupported Zn precursor prepared in a similar method at 200 °C for 4 h led to the formation of ZnO. But no diffraction peaks arising from ZnO appeared in the XRD spectra of ZnO/SiO_2 and $Au/ZnO/SiO_2$ catalysts, indicating high dispersion of ZnO on SiO_2. The Au(111) diffraction peak was observed in the XRD spectra of Au/SiO_2 and $Au/ZnO/SiO_2$-NH_3, but not in the XRD spectrum of $Au/ZnO/SiO_2$-Na_2CO_3. This indicates that the average crystalline size of Au nanoparticles was the finest in $Au/ZnO/SiO_2$-Na_2CO_3. From the XRD results, the average crystalline sizes of Au nanoparticles were calculated as 5 nm in $Au/ZnO/SiO_2$-NH_3 and 12 nm in Au/SiO_2. These XRD results demonstrate that the modification of SiO_2 with a small amount of ZnO facilitated the deposition of fine Au nanoparticles by DP using $HAuCl_4$ as the precursor.

Fig. 3 shows typical TEM images of the Au/SiO_2, $Au/ZnO/SiO_2$-NH_3, and $Au/ZnO/SiO_2$-Na_2CO_3 catalysts. The Au nano-

particles in Au/SiO_2 exhibited a wide size distribution from 5 to >20 nm. The Au nanoparticles in $Au/ZnO/SiO_2$-Na_2CO_3 showed a quite narrow size distribution of 2–7 nm, whereas those in $Au/ZnO/SiO_2$-NH_3 had a much wider distribution of 2 to >10 nm. We measured the size of more than 100 Au nanoparticles for each catalyst and plotted the particle size distributions in various catalysts (Fig. 3), from which we calculated the average size of the Au nanoparticles to be 10.4 nm in Au/SiO_2, 5.0 nm in $Au/ZnO/SiO_2$-NH_3, and 3.7 nm in $Au/ZnO/SiO_2$-Na_2CO_3. These results are in agreement with the XRD results. We further analyzed the elemental compositions of areas A, B, and C indicated in Figs. 3b, 3c, and 3d by EDS. Area A in $Au/ZnO/SiO_2$-NH_3 was with supported Au aggregates of ca. 10 nm, and area B in $Au/ZnO/SiO_2$-NH_3 and area C in $Au/ZnO/SiO_2$-Na_2CO_3 were with supported fine Au nanoparticles of 3–5 nm. The EDS results in Fig. 3 demonstrate an Au/Zn atomic ratio of 3.8 in area A, much higher than that in area B (0.36) and area C (0.42). This implies that Au nanoparticles were more highly dispersed in areas with a lower Au/Zn ratio in the catalysts.

The foregoing results demonstrate that fine Au nanoparticles in $Au/ZnO/SiO_2$-NH_3 and $Au/ZnO/SiO_2$-Na_2CO_3 were stabilized by ZnO supported on SiO_2, and thus the strong Au–ZnO interaction should be expected. We measured the PL spectra of various samples excited by the 366-nm laser that produced the strongest PL intensity (Fig. 4). ZnO/SiO_2 exhibited a broad and asymmetric luminescence band centered at 437 nm. The bulk ZnO showed typical emissions of narrow UV and broad green bands centered at ∼375 and ∼530 nm, respectively. Whereas the UV emission corresponded to the near band-edge emission, the green emission (commonly called a trap-state emission) resulted from the singly ionized oxygen vacancy in ZnO [24]. A violet emission of ZnO centered at ∼430 nm was reported previously [25–28], but its origin is not clear. Jin et al. proposed that this violet PL band is related to a luminescence center as the interface trap in the grain boundaries of ZnO_x crystals [26]. The broad and asymmetric luminescence band observed in ZnO/SiO_2 may be attributed to the addition of a major violet emission centered at 437 nm and a green shoulder centered at 525 nm. It is reasonable that ZnO highly dispersed on SiO_2 may have had a large grain boundary area and thus grain boundary defects. The intensity of ZnO/SiO_2 luminescence was dramatically suppressed after the loading of Au, clearly demonstrating the existence of a direct Au–ZnO interaction that enabled the nonirradiative relaxation of excitons formed in ZnO. As inferred from the relative luminescence intensities of ZnO in $Au/ZnO/SiO_2$-NH_3 and $Au/ZnO/SiO_2$-Na_2CO_3, the Au–ZnO interaction in $Au/ZnO/SiO_2$-Na_2CO_3 might be stronger than that in $Au/ZnO/SiO_2$-NH_3.

The Au 4f and Zn 3p XPS spectra of various catalysts are presented in Fig. 5A. It can be seen that the XPS peak of Au 4f partially overlaps with that of Zn 3p. Fig. 5B displays the Au 4f XPS spectra after the Zn 3p component was subtracted from the spectrum. It is noteworthy that great caution was taken during the XPS measurements to avoid a differential charge on the samples, with the requirement that the acquired Si 2p and O 1s spectra (not shown) must be symmetric. The results of the

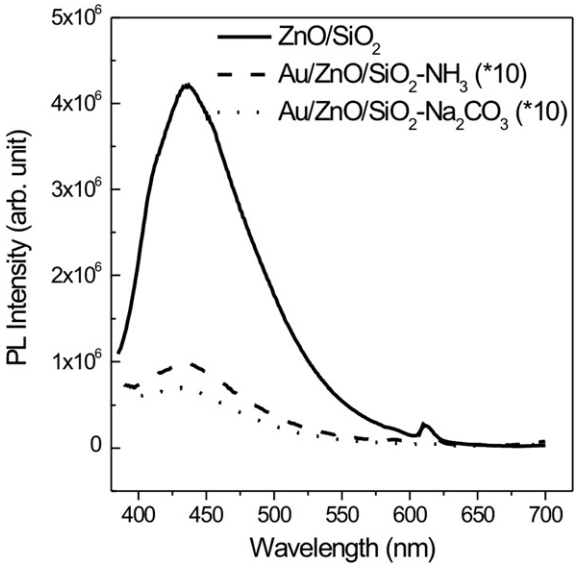

Fig. 4. PL spectra of various catalysts excited by the laser at 366 nm.

peak fitting of these spectra are summarized in Table 2. During the peak fitting process, the peak shapes for the Au 4f component were first acquired by fitting the XPS spectra of Au/SiO_2 catalyst, and then used to fit the Au 4f components in the XPS spectra of $Au/ZnO/SiO_2$. The Au 4f XPS spectrum of Au/SiO_2 could be fit with one component exhibiting its Au $4f_{7/2}$ binding energy at 83.8 eV, a typical value for metallic Au. However, the Au 4f XPS spectrum of $Au/ZnO/SiO_2$-NH_3 could be fitted satisfactorily only with two components with Au $4f_{7/2}$ binding energies of 83.7 and 85.5 eV, and that of $Au/ZnO/SiO_2$-Na_2CO_3 also could be fitted only with two components with Au $4f_{7/2}$ binding energies of 83.5 and 85.1 eV. These results indicate that two kinds of Au species exist in $Au/ZnO/SiO_2$ catalysts, one of which is metallic Au exhibiting the lower Au $4f_{7/2}$ binding energy.

We further investigated the electronic structure of various catalysts by XAS. Fig. 6 shows the Au L_{III}-edge XANES spectra of various catalysts. Au/SiO_2 demonstrated an adsorption edge at 11,919 eV, a shoulder at 11,933 eV (B), and two peaks at 11,949 (C) and 11,973 eV (D) in the Au L_{III}-edge XANES spectrum. These features are characteristic of the XANES spectrum of metallic Au [29,30], demonstrating that the Au in Au/SiO_2 was metallic Au, in agreement with the XPS results. The Au L_{III}-edge XANES spectra of $Au/ZnO/SiO_2$-NH_3 and $Au/ZnO/SiO_2$-Na_2CO_3 also exhibited the foregoing features arising from metallic Au, but with greatly differing intensities. The intensity of the metallic Au peaks in the XANES spectra of these catalysts followed the order Au/SiO_2 > $Au/ZnO/SiO_2$-NH_3 > $Au/ZnO/SiO_2$-Na_2CO_3, the reverse of the order for Au particle size. It was previously observed that the peak intensities in the XANES spectrum of Au nanoparticles decreased with the reducing particle size, which was attributed to an increased d-electron density of Au atoms in very small Au particles [31,32].

The Au L_{III}-edge XANES spectra of $Au/ZnO/SiO_2$-NH_3 and $Au/ZnO/SiO_2$-Na_2CO_3 exhibited a strong peak at 11,921.6 eV, whereas that of Au/SiO_2 did not. This feature corresponds to the white line position of Au due to a $2p_{3/2} \rightarrow 5d$ transition, with

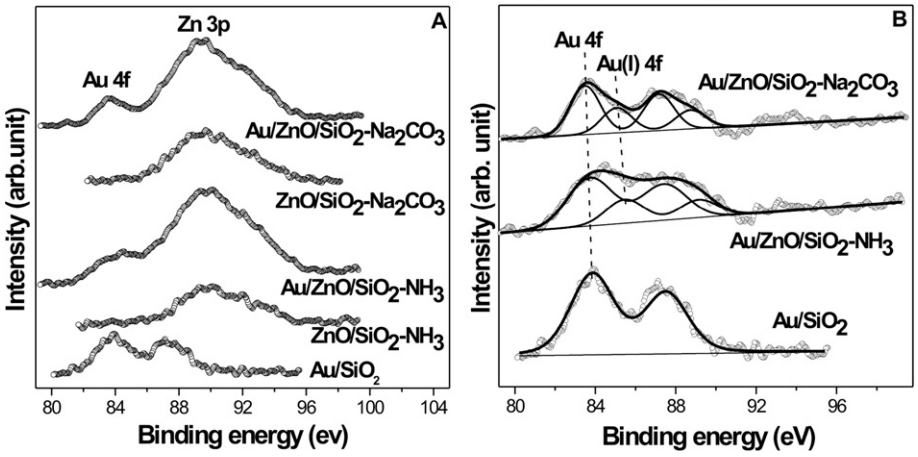

Fig. 5. (A) Au 4f and Zn 3p XPS spectra of various catalysts and (B) Au 4f XPS spectra after subtracting the Zn 3p component from the spectra. The scatter points and solid lines correspond to original data and fitting results, respectively. $h\nu = 1486.6$ eV.

Table 2
Peak-fitting results of XPS spectra of various catalysts

Catalyst	Au $4f_{7/2}$ (eV)		Au(I) $4f_{7/2}$ (eV)		Au:Au(I) peak area ratio
	BE[a]	FWHM[b]	BE	FWHM	
Au-SiO_2	83.8	2.56	–	–	–
Au/ZnO/SiO_2-NH_3	83.7	2.67	85.5	2.20	2.5:1
Au/ZnO/SiO_2-Na_2CO_3	83.5	1.76	85.1	1.76	1.9:1

[a] BE: binding energy.
[b] FWHM: full-width at half maximum.

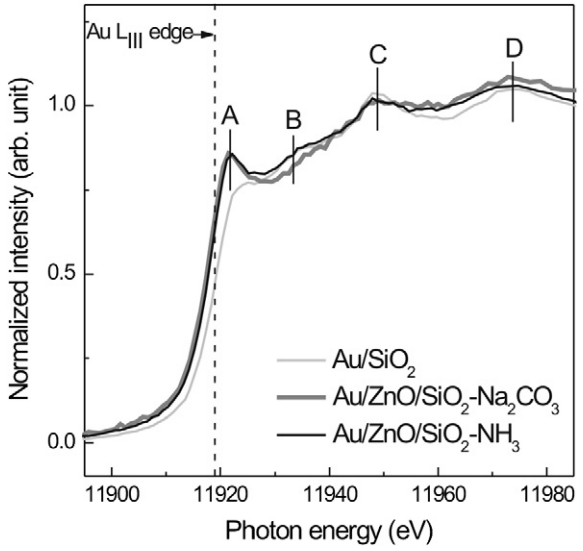

Fig. 6. Au L_{III}-edge XANES spectra of various catalysts.

its intensity proportional to that of unoccupied d states, which thus decreased with the reduced oxidation state of Au [33,34]. Therefore, the appearance of the intense feature at 11,921.6 eV in the Au L_{III}-edge XANES spectra of Au/ZnO/SiO_2-NH_3 and Au/ZnO/SiO_2-Na_2CO_3 clearly demonstrates the existence of Au cations [Au(I) or Au(III)] in these two catalysts. The XANES spectrum of Au(I) was similar to that of Au(III), but with an intermediate white line intensity. Comparing our XANES spectra with those reported in the literature [35], we

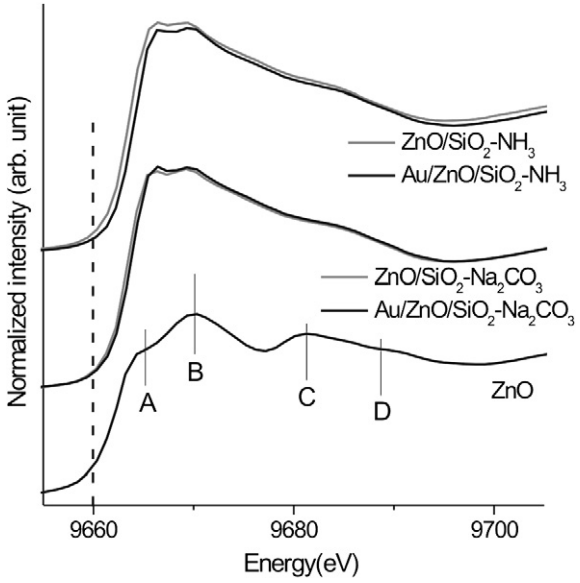

Fig. 7. Zn K-edge XANES spectra of various catalysts. The vertical dot line indicates the Zn K-edge at 9660 eV.

can assign our observed strong white line peak to Au(I) in Au/ZnO/SiO_2-NH_3 and Au/ZnO/SiO_2-Na_2CO_3; therefore, the Au species with an Au $4f_{7/2}$ binding energy at ~85.2 eV observed on XPS can be assigned to Au(I). The relative intensity of the Au(I) feature in Au/ZnO/SiO_2-NH_3 and Au/ZnO/SiO_2-Na_2CO_3 indicates a larger fraction of Au(I) in Au/ZnO/SiO_2-Na_2CO_3, in agreement with the XPS results (Table 2).

We also recorded the Zn K-edge XANES spectra of these catalysts (Fig. 7). ZnO powder prepared by calcining $Zn(NO_3)_2 \cdot 6H_2O$ at 400 °C for 4 h was chosen as the reference. The Zn K-edge XANES spectrum of ZnO showed a series of features (A–D) that can be assigned to the electron transitions from 1s- to 4p-derived empty states of Zn^{2+} in the wurtzite ZnO [36]. ZnO/SiO_2-NH_3 and ZnO/SiO_2-Na_2CO_3 exhibited Zn K-edge XANES spectra quite different from that of the ZnO powder, indicating that the local structure (especially the coordination symmetry) of ZnO supported on SiO_2 differs greatly from that in bulk ZnO. Interestingly, the loading of Au onto ZnO/SiO_2

also resulted in some change in the Zn K-edge XANES spectra. Although we cannot explain in detail the origin of the differences in the Zn K-edge XANES spectra of these catalysts, these results do imply that the Au–ZnO interaction in Au/ZnO/SiO_2 catalysts was sufficiently strong to exert some effect on the local structure of ZnO.

4. Discussion

4.1. Effect of the Au–ZnO interaction on the structures of Au and ZnO in Au/ZnO/SiO_2 catalysts

The current results, together with our previous results [18], demonstrate that SiO_2 modified by small amounts of transitional metal oxides can be used as the support for Au nanoparticles active in low-temperature CO oxidation. Moreover, the catalyst preparation can be conveniently accomplished by routine DP using $HAuCl_4$ as the precursor, thereby avoiding the use of complicated procedures and uncommon Au compounds. Thus, the Au/MO_x (e.g., M = Co, Zn)/SiO_2 catalysts may have potential practical applications. The DP agent used in catalyst preparation affects the performance of the resulting catalysts. An aqueous solution of Na_2CO_3 was a better DP agent than ammonium hydroxide for the preparation of Au/ZnO/SiO_2 catalysts. Au/ZnO/SiO_2-Na_2CO_3 demonstrated much better catalytic performance in low-temperature CO oxidation than Au/ZnO/SiO_2-NH_3. The Au:Zn:SiO_2 weight ratio was 1.55:4.8:100 in Au/ZnO/SiO_2-NH_3 and 1.12:6:100 in Au/ZnO/SiO_2-Na_2CO_3, respectively. Because ZnO on SiO_2 acts as the anchor for fine Au nanoparticles in Au/ZnO/SiO_2 catalysts, a high Zn:Si ratio should facilitate the high dispersion of Au nanoparticles. Our XRD and TEM results clearly demonstrate that Au nanoparticles were more highly dispersed in Au/ZnO/SiO_2-Na_2CO_3 than in Au/ZnO/SiO_2-NH_3.

A unique feature of the Au/ZnO/SiO_2 catalysts is that the inert SiO_2 is the major component and the loadings of active components Au and ZnO are comparable. Therefore, the interaction between the active components (i.e., the Au–ZnO interaction) can be manifested by the physical chemistry properties of both Au and ZnO in the catalysts. Our results clearly demonstrate that both the structure of Au nanoparticles and the local structure of ZnO are greatly affected by the Au–ZnO interaction. The former has been addressed frequently, but the latter has seldom been reported. In Au/ZnO catalysts, because ZnO interacting with Au represents only a very small fraction of the total ZnO support, the structural variation induced by the Au–ZnO interaction could not be observed. ZnO in ZnO/SiO_2 exhibits strong visible luminescence, but the luminescence of ZnO in Au/ZnO/SiO_2 is mostly quenched by the Au–ZnO interaction. Because the visible luminescence of ZnO is due to the oxygen vacancies and grain boundary defects, it can be reasonably deduced that Au nanoparticles should nucleate and locate on the oxygen vacancies and grain boundary defects of ZnO supported on SiO_2. It has been well established in model catalytic systems that Au nanoparticles nucleate on the defects on oxide surfaces; direct evidence of this is provided by the XANES results probing the local structures of materials. The Zn K-edge XANES spectra of ZnO in bulk ZnO, ZnO/SiO_2 supports, and Au/ZnO/SiO_2 catalysts differ substantially. XPS results demonstrate that Zn exists in Zn(II) in these samples, therefore, different XANES spectra indicate different local structures of ZnO species. The bulk ZnO is with a local structure of wurtzite. ZnO in ZnO/SiO_2 is highly dispersive and has abundant oxygen vacancies and grain boundary defects, resulting in a local structure of ZnO that differs from that of bulk ZnO. Meanwhile, the interaction between ZnO and SiO_2 in ZnO/SiO_2 also may partially distort the local structure of Zn(II) from the $[ZnO_4]^{6-}$ tetrahedral unit in bulk ZnO to the ZnO_4 tetrahedra linking to surrounding silicate tetrahedral in crystalline Zn silicates [37]. The Zn K-edge XANES spectra of Au/ZnO/SiO_2-NH_3 and Au/ZnO/SiO_2-Na_2CO_3 differ obviously (albeit only slightly) from those of ZnO/SiO_2-NH_3 and ZnO/SiO_2-Na_2CO_3. This implies that the Au–ZnO interaction does exist in the catalysts and can affect the local structure of ZnO. Therefore, our results clearly demonstrate the influence of the Au–ZnO interaction on the local structure of ZnO.

It has been established that the Au–support interaction determines the structure of supported Au nanoparticles. Our results provide some new and interesting insights. Our average Au nanoparticle sizes of 10.4 nm in Au/SiO_2, 5.0 nm in Au/ZnO/SiO_2-NH_3, and 3.7 nm in Au/ZnO/SiO_2-Na_2CO_3 indicate that ZnO was more capable of stabilizing fine Au nanoparticles than SiO_2. This may be due to the more abundant vacancies on transitional metal oxides compared with on SiO_2. Our findings demonstrate that the stability of fine Au nanoparticles on ZnO interaction depends on the local Au:Zn ratio. Our TEM results showed a wide size distribution of Au nanoparticles in Au/ZnO/SiO_2-NH_3, and our EDS analysis demonstrated that a low Au/Zn ratio facilitated the formation of fine Au nanoparticles. The Au/Zn atomic ratio was ∼0.4 in areas with fine Au nanoparticles in both Au/ZnO/SiO_2-NH_3 and Au/ZnO/SiO_2-Na_2CO_3, increasing to 3.8 in areas with Au aggregates in Au/ZnO/SiO_2-NH_3. These results imply that certain amounts of ZnO are required to stabilize supported fine Au nanoparticles, or otherwise these fine Au nanoparticles will aggregate. Similar results have been observed in the Au/TiO_2(110) model catalytic system. In a combined STM and DFT study of Au growth on TiO_2(110) at 300 K in which a bimodal size distribution of Au clusters was observed, the authors proposed that Au cluster nucleates primarily at oxygen vacancy sites, but that with further growth, a single oxygen vacancy can no longer stabilize the cluster, and the cluster–vacancy complex will then diffuse [38]. While diffusing, the cluster–vacancy complex will either encounter other surface defects to be stabilized on the surface or encounter another cluster, eventually leading to agglomeration [38].

Our XANES and XPS results clearly demonstrate the coexistence of metallic Au and Au(I) in Au/ZnO/SiO_2-NH_3 and Au/ZnO/SiO_2-Na_2CO_3. Previous infrared studies have found both metallic and oxidized Au clusters in Au/ZnO catalysts [39]. An interesting result here is the core-level binding energy of metallic Au nanoparticles in these catalysts. The average size and the Au $4f_{7/2}$ core-level binding energy of

Au nanoparticles in these catalysts followed the same order: Au/SiO_2 > $Au/ZnO/SiO_2$-NH_3 > $Au/ZnO/SiO_2$-Na_2CO_3. But it generally is observed that the Au 4f core-level binding energy of supported metallic Au nanoparticles increases with the decreasing particle size, the origin of which remains unclear [40]. Thus, our XPS results indicate that a charge transfer must occur from ZnO to metallic Au nanoparticles, thereby reducing the core-level binding energy of Au nanoparticles; that is, fine Au nanoparticles are partially negatively charged in $Au/ZnO/SiO_2$-NH_3 and $Au/ZnO/SiO_2$-Na_2CO_3. Otherwise, Au nanoparticles of much finer sizes in $Au/ZnO/SiO_2$-NH_3 and $Au/ZnO/SiO_2$-Na_2CO_3 should exhibit higher core-level binding energies than those in Au/SiO_2 because of their different particle sizes. Oxygen vacancies on transitional metal oxides on which Au clusters nucleate are capable of charge transfer to supported Au clusters [41].

Of the catalysts studied, Au/SiO_2 exhibited catalytic activity only at reaction temperatures above 543 K, $Au/ZnO/SiO_2$-NH_3 showed some activity at low reaction temperatures, and $Au/ZnO/SiO_2$-Na_2CO_3 exhibited the best catalytic performance, achieving 100% CO conversion at 303 K. Unlike reducible transitional metal oxides, ZnO cannot participate in the catalytic CO oxidation; thus, the observed catalytic activity can be related only to the structure of Au nanoparticles in the catalysts determined by the Au–ZnO interaction. Our results agree with the general activity–size dependence of supported metallic Au nanoparticles in CO oxidation. The fraction of low-coordinated Au atoms on Au nanoparticles increases with decreasing particle size, and these low-coordinated Au atoms are active in low-temperature CO oxidation [42]. Meanwhile, charge transfer occurs from ZnO to fine Au nanoparticles, which also enhances the activity of metallic Au nanoparticles in CO oxidation [40]. Our results also demonstrate the existence of Au(I) in $Au/ZnO/SiO_2$ catalysts, with a higher Au(I)/Au ratio in $Au/ZnO/SiO_2$-Na_2CO_3 than in $Au/ZnO/SiO_2$-NH_3. The role of Au(I) species in CO oxidation remains unclear. Although Boccuzzi et al. reported the existence of Au(I) species in Au/ZnO catalyst [39], Au(I) species was not involved in their proposed reaction mechanism of CO oxidation over Au/ZnO [43]. However, theoretical calculations showed that Au(I) can be stabilized on the vacancy sites of ZnO, and that CO adsorbs most strongly on Au(I) in Au/ZnO [44].

4.2. *Reaction mechanism of CO oxidation catalyzed by $Au/ZnO/SiO_2$ catalysts*

An uncommon but interesting phenomenon is the activity–reaction temperature dependence observed in CO oxidation over $Au/ZnO/SiO_2$-NH_3. The used catalyst showed the same activity–reaction temperature dependence as the fresh catalyst, demonstrating that the active structure of Au nanoparticles did not change during the course of catalytic reaction. Therefore, the activity decrease seen between 363 and 453 K must not be due to the change in the active structure in the catalyst. Similar experimental results have been reported previously [17,45,46]. Wang et al. studied Au–Ag alloy nanoparticles supported on a mesoporous support as a catalyst for CO oxidation and found that the catalytic activity decreased between 40 and 160 °C and increased thereafter [45]. Zhu et al. also observed a similar phenomenon in their Au/SiO_2 catalysts for CO oxidation prepared from the cationic Au precursor [17]. But these two groups gave no explanation for this phenomenon in their papers. Daté et al. studied the role of moisture in the catalytic activity of Au/SiO_2 catalyst prepared by gas-phase grafting in CO oxidation [46]. At a moderate moisture concentration in the reaction gas, a temperature window was observed in which CO conversion first decreased and then increased with increasing reaction temperature [46]. The activity decrease was attributed to desorption of moisture from the catalyst surface, which plays an important role in the catalytic activity of Au/SiO_2 catalyst in low-temperature CO oxidation [46].

The influence of moisture can be excluded in the present study, however, because the reaction gas consisted of CO and dry air with a water content below 5 ppm. Furthermore, $Au/ZnO/SiO_2$-Na_2CO_3 did not exhibit the activity–reaction temperature dependence seen for $Au/ZnO/SiO_2$-NH_3. We speculate that the observed activity–reaction temperature dependence indicates that CO oxidation over $Au/ZnO/SiO_2$ follows different mechanisms at low and high reaction temperatures. At high reaction temperatures, CO oxidation follows the LH mechanism on the Au surface, in which oxygen adatoms result from a direct oxygen dissociation reaction with adsorbed CO to form CO_2. In this mechanism, oxygen dissociation (an activation process) is the rate-limiting step, which is reasonably facilitated at elevated temperatures. The Au particle size has a significant influence on oxygen dissociation; it is generally believed that the barrier of oxygen dissociation on fine Au nanoparticles is substantially lower. Theoretical calculation results indicate that oxygen dissociation on small Au particles may be possible when Au is low-coordinated [47]; therefore, the barrier for CO oxidation catalyzed by Au particles following the high-temperature reaction mechanism decreases with decreasing Au particle size. With decreasing reaction temperature, the probability of oxygen dissociation on the Au surface decreases, and the high-temperature reaction pathway of CO oxidation becomes blocked. The temperature at which the high-temperature reaction pathway will become completely blocked depends mainly on the structure and size of the Au nanoparticles.

The activity of $Au/ZnO/SiO_2$-NH_3 in CO oxidation at low temperatures (300–450 K) follows a different mechanism than the high-temperature reaction mechanism. We propose that a characteristic of the low-temperature reaction mechanism is that oxygen does not undergo direct dissociation on the Au surface. Several reaction pathways have been proposed to account for the exceptional activity of fine Au nanoparticles in low-temperature CO oxidation, including CO oxidation by molecularly adsorbed oxygen and involvement of surface hydroxyls in CO oxidation [40]. Our results provide no information on the detailed reaction mechanism, but the observed “volcano” shape of the activity–reaction temperature dependence strongly suggests that a weakly chemisorbed species, the nature of which remains to be identified, is the key active species. The formation of this weakly chemisorbed species is facilitated over fine

Au nanoparticles. At low reaction temperatures, the coverage of this weakly chemisorbed species initially increases with increasing reaction temperature, resulting in an initial increase in catalytic activity. But with further increases in reaction temperature, desorption of this weakly chemisorbed species occurs, and eventually the weakly chemisorbed species cannot form on the surface; thus, the catalytic activity decreases. Therefore, it is the competition between desorption and surface reaction of the weakly chemisorbed species that leads to the observation of a local maximum catalytic activity with increasing temperature at low reaction temperatures.

Based on the foregoing discussion, the apparent activity of supported Au nanoparticles in CO oxidation consists of contributions from CO oxidation following both the low-temperature and high-temperature reaction mechanisms. Intrinsically, the activity of supported Au nanoparticles following the low-temperature reaction mechanism must exhibit a "volcano" dependence on the reaction temperature, whereas that following the high-temperature reaction mechanism increases monotonically with increasing reaction temperature; however, both activities increase with decreasing Au particle size. There should be a temperature window in which the reaction mechanism switches from the low-temperature to the high-temperature reaction mechanism; however, whether or not this temperature window can be observed experimentally depends on the catalyst. For highly active Au catalysts such as $Au/ZnO/SiO_2$-Na_2CO_3, with increasing reaction temperature, the activity loss contributed by the low-temperature reaction mechanism can be effectively compensated for by the activity gain contributed by the high-temperature reaction mechanism, and thus no apparent loss of activity can be observed. Because of the particular catalyst structure of $Au/ZnO/SiO_2$-NH_3, such a temperature window was observed, demonstrating the existence of different reaction mechanisms of CO oxidation catalyzed by supported Au nanoparticles.

5. Conclusion

We have demonstrated that, using $HAuCl_4$ as precursor, the convenient DP method can deposit fine Au nanoparticles on SiO_2 modified with a small amount of highly dispersed ZnO. The resulting $Au/ZnO/SiO_2$ catalysts are active in low-temperature CO oxidation. Fine Au nanoparticles are mostly supported on ZnO on SiO_2. Aqueous solution of Na_2CO_3 is a better DP agent than ammonium hydroxide. Strong Au–ZnO interactions exist in the catalysts and exert a significant influence on the structures of both Au nanoparticles and ZnO. Our results suggest that CO oxidation over supported Au nanoparticles follows different mechanisms at low and high reaction temperatures and that a weakly chemisorbed species is involved in low-temperature CO oxidation. These results deepen our fundamental understanding of CO oxidation catalyzed by supported Au nanoparticles. Our synthesis strategy provides a practical approach for using commercially favorable SiO_2 as the support for active supported Au catalysts.

Acknowledgments

This work was supported by the National Natural Science Foundation of China (Grant 20503027), the "Hundred Talent Program" of the Chinese Academy of Sciences, the MOE program for PCSIRT (IRT0756), and the MPG-CAS partner group.

References

[1] G.C. Bond, D.T. Thompson, Catal. Rev.-Sci. Eng. 41 (1999) 319.
[2] M. Haruta, M. Daté, Appl. Catal. A 222 (2001) 427.
[3] G.J. Hutchings, M. Hurata, Appl. Catal. A 291 (2005) 2.
[4] A.S.K. Hashmi, G.J. Hutchings, Angew. Chem. Int. Ed. 45 (2006) 7896.
[5] M. Haruta, T. Kobayashi, H. Sano, N. Yamada, Chem. Lett. 16 (1987) 405.
[6] G.C. Bond, D.T. Thompson, Gold Bull. 33 (2000) 41.
[7] M.C. Kung, R.J. Davis, H.H. Kung, J. Phys. Chem. C 111 (2007) 11767.
[8] M.M. Schubert, S. Hackenberg, A.C. van Veen, M. Muhler, V. Plzak, R.J. Behm, J. Catal. 197 (2001) 113.
[9] M. Okumura, S. Nakamura, S. Tsubota, T. Nakamura, M. Azuma, M. Haruta, Catal. Lett. 51 (1998) 53.
[10] M.A.P. Dekkers, M.J. Lippits, B.E. Nieuwenhuys, Catal. Today 54 (1999) 381.
[11] S.H. Overbury, L. Ortiz-Soto, H. Zhu, B. Lee, M.D. Amiridis, S. Dai, Catal. Lett. 95 (2004) 99.
[12] J. Chou, N.R. Franklin, S.H. Baeck, T.F. Jaramillo, E.W. McFarland, Catal. Lett. 95 (2004) 107.
[13] K. Qian, Z.Q. Jiang, W.X. Huang, J. Mol. Catal. A 264 (2007) 26.
[14] M. Okumura, S. Tsubota, M. Haruta, J. Mol. Catal. A 199 (2003) 73.
[15] G. Budroni, A. Corma, Angew. Chem. Int. Ed. 45 (2006) 3328.
[16] H.G. Zhu, C.D. Liang, W.F. Yan, S.H. Overbury, S. Dai, J. Phys. Chem. B 110 (2006) 10842.
[17] H.G. Zhu, Z. Ma, J.C. Clark, Z.W. Pan, S.H. Overbury, S. Dai, Appl. Catal. A 326 (2007) 89.
[18] K. Qian, W.X. Huang, Z.Q. Jiang, H.X. Sun, J. Catal. 248 (2007) 137.
[19] L. Guczi, K. Frey, A. Beck, G. Petõ, C.S. Daróczi, N. Kruse, S. Chenakin, Appl. Catal. A 291 (2005) 116.
[20] A.M. Venezia, F.L. Liotta, G. Pantaleo, A. Beck, A. Horváth, O. Geszti, A. Kocsonya, L. Guczi, Appl. Catal. A 310 (2006) 114.
[21] A. Horváth, A. Beck, A. Sárkány, G. Stefler, Z. Varga, G.O. Eszti, L. Tóth, L. Guczi, J. Phys. Chem. B 110 (2006) 15417.
[22] F. Boccuzzi, A. Chiorino, S. Tsubota, M. Haruta, Catal. Lett. 29 (1994) 225.
[23] G.Y. Wang, W.X. Zhang, H.L. Lian, D.Z. Jiang, T.H. Wu, Appl. Catal. A 239 (2003) 1.
[24] K. Vanheusden, W.L. Warren, C.H. Seager, D.R. Tallant, J.A. Voigt, B.E. Gnade, J. Appl. Phys. 79 (1996) 7983.
[25] S. Monticone, R. Tufeu, A.V. Kanaev, J. Phys. Chem. B 102 (1998) 2854.
[26] B.J. Jin, S. Im, S.Y. Lee, Thin Solid Films 366 (2000) 107.
[27] J.-J. Wu, S.-C. Liu, Adv. Mater. 14 (2002) 215.
[28] S.J. Chen, Y.C. Liu, Y.M. Lu, J.Y. Zhang, D.Z. Shen, X.W. Fan, J. Cryst. Growth 289 (2006) 55.
[29] M.P. Casaletto, A. Longo, A.M. Venezia, A. Martorana, A. Prestianni, Appl. Catal. A 302 (2006) 309.
[30] N. Weiher, E. Bus, L. Delannoy, C. Louis, D.E. Ramaker, J.T. Miller, J.A. van Bokhoven, J. Catal. 240 (2006) 100.
[31] J.T. Miller, A.J. Kropf, Y. Zha, J.R. Regalbuto, L. Delannoy, C. Louis, E. Bus, J.A. van Bokhoven, J. Catal. 240 (2006) 222.
[32] J.A. van Bokhoven, J.T. Miller, J. Phys. Chem. C 111 (2007) 9245.
[33] A. Pantelouris, G. Küper, J. Hormes, C. Feldmann, M. Jansen, J. Am. Chem. Soc. 117 (1995) 11749.
[34] J. Guzman, B.C. Gates, J. Phys. Chem. B 106 (2002) 7659.
[35] C.K. Costello, J. Guzman, J.H. Yang, Y.M. Wang, M.C. Kung, B.C. Gates, H.H. Kung, J. Phys. Chem. B 108 (2004) 12529.
[36] J.W. Chiou, J.C. Jan, H.M. Tsai, C.W. Bao, W.F. Pong, M.-H. Tsai, I.-H. Hong, R. Klauser, J.F. Lee, J.J. Wu, S.C. Liu, Appl. Phys. Lett. 84 (2004) 3462.

[37] H. Yoshida, T. Shimizu, C. Murata, T. Hattori, J. Catal. 220 (2003) 226.
[38] E. Wahlström, N. Lopez, R. Schaub, P. Thostrup, A. Rønnau, C. Africh, E. Laegsgaard, J.K. Nørskov, F. Besenbacher, Phys. Rev. Lett. 90 (2003) 026101.
[39] F. Boccuzzi, A. Chiorino, S. Tsubota, M. Haruta, Sens. Actuators B Chem. 24–25 (1995) 540.
[40] R. Meyer, C. Lemire, Sh.K. Shaikhutdinov, H.-J. Freund, Gold Bull. 37 (2004) 72.
[41] Z.Q. Jiang, W.H. Zhang, L. Jin, X. Yang, F.Q. Xu, J.F. Zhu, W.X. Huang, J. Phys. Chem. C 111 (2007) 12434.
[42] N. Lopez, T.V.W. Janssens, B.S. Clausen, Y. Xu, M. Mavrikakis, T. Bligaard, J.K. Nørskov, J. Catal. 223 (2004) 232.
[43] F. Boccuzzi, A. Chiorino, S. Tsubota, M. Haruta, J. Phys. Chem. 100 (1996) 3625.
[44] N.S. Phala, G. Klatt, V.E. an Steen, S.A. French, A.A. Sokol, C.R.A. Catlow, PCCP 7 (2005) 2440.
[45] A.Q. Wang, Y.P. Hsieh, Y.F. Chen, C.Y. Mou, J. Catal. 237 (2006) 197.
[46] M. Daté, M. Okumura, S. Tsubota, M. Haruta, Angew. Chem. Int. Ed. 43 (2004) 2129.
[47] N. Lopez, J.K. Norskov, J. Am. Chem. Soc. 124 (2002) 11262.